Systematics of pion absorption on ^{6}Li

R. D. Ransome, V. R. Cupps,* S. Dawson,† R. W. Fergerson,‡ and A. Green
Rutgers University, Piscataway, New Jersey 08855

C. L. Morris and J. A. McGill
Los Alamos National Laboratory, Los Alamos, New Mexico 87545

J. R. Comfort, B. G. Ritchie, and J. R. Tinsley
Arizona State University, Tempe, Arizona 85287

J. D. Zumbro§
University of Pennsylvania, Philadelphia, Pennsylvania 19104
and Los Alamos National Laboratory, Los Alamos, New Mexico 87545

R. A. Loveman**
University of Colorado, Boulder, Colorado 80309

P. C. Gugelot
University of Virginia, Charlottesville, Virginia 22901

D. L. Watson
University of York, York YO1 5DD, United Kingdom

C. Fred Moore
University of Texas at Austin, Austin, Texas 78712
(Received 22 May 1990)

Particle emission following π^+ absorption on ^{6}Li at $T_\pi = 50$, 100, 150, and 200 MeV was studied with a large-solid-angle detector. Evidence is found for a three-nucleon-absorption mode, which takes place predominantly on *pnn* triplets. This mode increases in importance from about a quarter of the absorption cross section at 50 MeV to about one-half at 200 MeV.

I. INTRODUCTION

Until about 1980 it was believed that pion absorption in nuclei was based on the elementary process which entails absorption on a deuteronlike (*pn*) pair, called quasideuteron absorption (QDA). This belief was challenged by McKeown *et al.*,[1] who suggested that absorption in nuclei might involve substantial energy sharing among three or more nucleons. This suggestion has been supported by several subsequent experiments.[2–12] Theoretical calculations have also indicated that about one-half of the absorption cross section could be attributed to direct multinucleon absorption in heavy nuclei.[13,14] There is now considerable interest in obtaining quantitative measures of these different mechanisms in order to provide a thorough understanding of pion interactions with nuclei.

Pion absorption that leads to multinucleon final states is difficult to measure because the conventional detectors frequently used in coincidence experiments typically have very small solid angles. Most experiments have used two detectors in the same scattering plane set at angles that correspond to the QDA process. Yields are typically reduced substantially for other angle pairs, and there are only a few limited measurements of noncoplanar cross sections. Thus previous experiments have not been very sensitive to multinucleon emission.

Estimates of the fraction of non-QDA absorption have normally come from measurements of the cross section for emission of two protons with quasideuteron kinematics which are then compared with values of the total absorption cross section. The observed cross sections are typically only a few percent of the total absorption cross sections for nuclei heavier than carbon. However, substantial corrections need to be made for a QDA process that is either preceded by a scattering of the pion before absorption, called an initial-state interaction (ISI), or followed by scatterings of the outgoing nucleons after the absorption, called a final-state interaction (FSI). Calculations based on intranuclear cascade models can provide estimates of the importance of ISI/FSI, but these models currently do not include off-shell effects, correlations between the nucleons, or any treatments of three-body absorption. The interpretation of the results is therefore

 ©1990 The American Physical Society

very uncertain.[14] In addition, the total cross sections are generally known only to within about 20%.

The clearest indications of multinucleon mechanisms have come from studies of ^{3}He (Refs. 5 and 7) and ^{4}He.[8,9,11] The experiments focused on the correlations between two outgoing nucleons, and a substantial fraction (10–30%) of the cross section was identified for which three nucleons had an energy distribution very much like phase space. These results were interpreted as an indication of a three-body absorption process. If true three-body absorption exists, it might well be dependent on the nuclear size or density and could be more (or possibly less) important in heavier nuclei. However, the separation of absorption from ISI/FSI processes becomes increasingly difficult as the number of nucleons increases. A systematic study of absorption in nuclei is required in order to untangle the absorption process in heavier nuclei.

We have conducted such a study on a variety of nuclei from ^{6}Li to ^{238}U for pion energies from 50 to 500 MeV, with emphasis on those final states that contain two or more energetic protons. We report here on the systematics of π^+ absorption on ^{6}Li leading to at least two energetic protons in the final state, for π^+ energies of 50, 100, 150, and 200 MeV. Some of these results at 150 MeV have been reported previously.[15] This is the first measurement on ^{6}Li of both three-proton coincidences as well as two-proton coincidences with no restrictions on coplanarity. In addition, coincidences of two protons with neutrons and deuterons have also been measured. The measurement of the ratios of three-particle coincidences to two-proton coincidences as a function of energy gives new information on the absorption mechanism and the importance of ISI/FSI. We will show that about one-third of the cross section leading to two or more energetic protons does not seem to be consistent with QDA and a single ISI/FSI.

Although there have been several other studies of pion absorption on ^{6}Li,[16–23] and some are in progress,[24,25] they have typically measured nearly coplanar two-proton or *pn* coincidences. Most have also been done for pion energies below 76 MeV, except for the works of Yokota *et al.*,[16–18] where the maximum energy was 165 MeV, Bressani *et al.*,[19] with energies up to 300 MeV, Zhang *et al.*[24] and Rothenberger *et al.*,[25] these latter two covering energies from 30 to 220 MeV.

II. EXPERIMENT

The experiment was performed with a new large-solid-angle detector at the Clinton P. Anderson Meson Physics Facility (LAMPF) of the Los Alamos National Laboratory, the BGO ball. The BGO ball consists of 30 phoswich detectors, each detector having a 3-mm-thick plastic scintillator optically coupled to the front of a 5.6-cm-thick bismuth germanate (BGO) crystal, with a 7.62-cm-diameter photomultiplier tube mounted on the back. The anode signal from the phototube is time sliced to provide both ΔE (fast) and E (slow) signals for charged particle identification of pions, protons, deuterons, etc., and for identification of neutrons and gamma rays. It was not possible to distinguish neutrons from gamma rays with these detectors. The crystals were thick enough to stop up to 185-MeV protons and 90-MeV pions. The time resolution of the detectors was about 1 ns, sufficient to eliminate events with hits from different beam bursts (the LAMPF beam has a 5-ns microstructure).

The 30 detectors cover $0.88 \times 4\pi$ sr of solid angle and span scattering angles from 26° to 161°. The target was placed one centimeter downstream of the center of the ball in this experiment, which accounts for the asymmetry in the angular coverage. Each detector had a solid angle of about $\frac{1}{32} \times 4\pi$ sr and was supported in a 0.5-mm-thick electro-formed nickel can which had a 0.05-mm-thick entrance window, with the support covering about 5% of the solid angle of each crystal.

The target was composed of 99% pure ^{6}Li, with a cross-sectional area of 1×2 cm and a thickness of 0.207 g/cm^2. The pion beam had an average intensity of a few 10^4/sec, allowing the beam particles to be counted. A 0.25-mm-thick plastic scintillator with a cross section of 0.5×0.5 cm^2 was located about one centimeter upstream of the target. A coincidence of this detector with another scintillator farther upstream and any two of the BGO crystals was used as the event trigger.

An initial energy scale was established from the energy-loss characteristics of protons and the thicknesses of the crystals. A detailed calibration was obtained from data taken for the $\pi^+ d \rightarrow 2p$ reaction with a CD_2 target. Small adjustments were made to other runs by comparing the ΔE vs E curve for each detector with that found from the CD_2 calibration. The calibration is believed to be accurate to about 5% or better. An energy resolution of 3% full width at half maximum (FWHM) was obtained at 238 MeV (100-MeV pions) for the total energy sum of protons, summed over all detectors in the ball. This width includes contributions from the momentum spread of the beam and energy-loss straggling in the target.

Ten scintillator sets were also placed downstream, with five to the left of the beam and five to the right. Each set consisted of three 10-cm-diameter, 10-cm-deep liquid scintillators and two plastic scintillators 7.3×7.7 cm^2 in area by 15-cm thick. A 1.1-cm-thick scintillator paddle was placed between each set and the target. The front faces of the paddles were located 2.5 m from the target and the nominal angles of each group of five sets were 8.2° to 14° in equal intervals. Although these devices were initially intended to detect neutrons, the background proved too high for a reasonable measurement. They were thus used only to detect protons in the forward direction, with the front paddle providing a ΔE signal and the thick scintillators an energy measurement. Pions and protons could thereby be separated, and the total energy was determined by a time-of-flight method. These detectors had a proton-energy threshold of about 40 MeV. They were not included in the trigger, and were only read out if other trigger conditions were met.

The observed particles were divided into six groups: protons, deuterons, low-energy charged particles, high-energy neutrals, low-energy neutrals, and pions. Protons with energies below 18 MeV stopped in the plastic scintillator and could not be distinguished from other charged particles that stopped in the plastic. A lower limit of 22 MeV on the detected energy was used in the analysis in order to assure a clear identification of the protons. In the following discussions a "proton" will thus mean an event with an observed energy greater than 22 MeV in the detectors. Neutrals with an observed energy less than 18 MeV were classified as low-energy neutrals in order to help separate low-energy gamma rays and noise from neutrons. All particles with less than 0.5-MeV observed energy in the plastic and no signal in the BGO were also placed in the low-energy-neutral category. Charged particles that stopped in the plastic scintillator, or which fell on the proton line between 18 and 22 MeV, were placed in the low-energy charged-particle category.

One thickness of the target (0.2 g/cm^2) could stop a 12-MeV proton, and one cm (the half height of the target) could stop an 18-MeV proton. A proton with an observed energy of 22 MeV corresponds to a proton energy of about 25 MeV before energy loss in the target. The spectra shown later do not contain any corrections for energy loss in the target, although such corrections were made for the simulations described in Secs. III and IV.

III. RESULTS

In order to facilitate comparisons of these data with future measurements and theoretical calculations, we wish to divide the discussion into two parts. Section III will present the observed cross sections, discuss the general features of the data, and discuss corrections required to estimate the total cross sections for various final states. Section IV will describe the applications of a phase-space model. Comparisons between the results of the model and the angular dependence of the proton spectra will be made, and implications regarding the absorption process will be assessed.

A. Cross sections

The bulk of the observed absorption cross section includes two or three energetic protons in the final state. For purposes of discussion, the multiproton events have been divided into two categories: those with two observed protons and those with three observed protons. Thus two-proton inclusive events are all those events with two and only two observed protons that each have at least 22-MeV observed energy, plus possible neutrons, deuterons, or low-energy charged particles, but not containing an identified pion. Three-proton inclusive events are defined similarly. The four-proton inclusive final channel had very small measured cross sections, consistent with zero and never greater than 0.1 mb. In addition, neutrons and deuterons were also observed in coincidence with one to three protons. Listings of the observed inclusive cross sections, without corrections described below, are given in Tables I and II.

In spite of the large solid angle of the BGO ball, substantial cross section was missed for various reasons. About $\frac{2}{32}$ of the full solid angle was not covered due to the beam entrance and exit holes. The importance of this omission depends on the degree to which a reaction is forward (or backward) peaked. In addition, about 5% of the solid angle inside the ball was blocked by the support cans. At higher energies, losses due to nuclear reactions and to scattering out of the crystals into the support cans became important, with the losses estimated to be about 30% for 200-MeV protons. The energy threshold for proton identification is relatively more important for three-body absorption and for pions at low incident energy.

Corrections for the losses due to blocked solid angle and for nuclear reactions in the ball are relatively simple, while corrections for the missing-solid-angle and threshold effects require a model for the interaction. We have used a phase-space model, which will be described in Sec. IV, as the basis for these latter corrections.

Comparisons between different runs with the same target and between the $\pi^+ d \rightarrow 2p$ cross section and the p-shell absorption on ^{6}Li, which is known to be about 95% of the deuteron absorption cross section,[20] indicated that the systematic errors are less than 10%. Estimates of the total $\pi^+ d \rightarrow 2p$ cross section, including all corrections, were within 15% of values obtained from an accepted parametrization.[26] The statistical errors on the

TABLE I. Measured and corrected cross sections under various constraints. The "2p inclusive" and "3p inclusive" values are observed cross sections for reactions leading to two and three detected protons, respectively. All other entries are estimated total cross sections derived from correction procedures discussed in the text. The values 18 and 25 MeV indicate the detection threshold for protons (reaction energies before energy loss in the target), "ball" indicates the cross section within the angular coverage of the BGO ball, and "all" indicates the estimate for the full solid angle. The "3p total" entry is the total estimated cross section leading to three free protons with no threshold, and "total" is the total estimated cross section leading to two or more free protons.

	50 mb	100 mb	150 mb	200 mb
2p inclusive	16	30	36	31
2p 25-MeV ball	22	40	50	40
2p 25-MeV all	28	50	61	48
2p 18-MeV all	30	51	62	47
3p inclusive	0.22	1.2	2.6	3.8
3p 25-MeV ball	0.31	1.6	3.8	5.9
3p 25-MeV all	0.42	2.2	5.0	7.8
3p 18-MeV ball	0.64	2.6	5.5	7.6
3p 18-MeV all	0.85	3.3	7.1	9.8
3p total	1.9	9.3	14	21
Total	32	60	76	68

TABLE II. Measured cross sections leading to two and three protons in coincidence with other particles. The final row gives the cross sections for final states with two or more charged particles (except pions) and at most one neutral, and which do not contain two or more protons or one proton and one deuteron. The $2p$ and $3p$ inclusive cross sections are given in Table I.

	50 mb	100 mb	150 mb	200 mb
$2p$ exclusive	15	25	28	21
$2p$ deuteron	0.3	0.9	1.4	1.4
$2p$ neutron	0.06	0.4	1.4	3.1
$2p$ low charged	1.2	3.0	4.4	4.0
$3p$ exclusive	0.21	1.0	2.2	3.2
$1p$ one deuteron	2.4	3.6	3.6	3.7
$2p\pi$	0.03	0.07	0.45	1.4
Two charged	7.0	10	14	14

cross sections were much smaller, usually around 1%, so we have not included the statistical error in the quoted cross sections. The cross sections should thus be understood to have a systematic uncertainty of about 10% for the empirical values, and about 15% for the corrected values.

The corrected cross sections for two-proton and three-proton inclusive final states are given in Table I, along with estimates for the total cross sections. All of these cross sections include corrections for nuclear reactions and losses in the support cans. Corrections for the detected energy threshold were made on the basis of the phase-space model with a threshold value of 25 MeV from the reaction (before energy loss in the target). Separate cross sections with and without corrections for the missing solid angle in the beam direction are given.

As an indication of the sensitivity to threshold, we also give the estimated cross sections with a threshold of 18 MeV (before energy loss in the target) as well as extrapolations to zero threshold. As a consequence of the use of a phase-space model, the estimated portion of the three-proton final state that is seen as two protons depends on the detection threshold. This fact is seen clearly for the 200-MeV data where lowering the threshold actually decreases the two-proton cross section, because less of the three-proton cross section is seen as two protons. The extrapolation to zero threshold is least certain for the three-proton case. If one proton has a momentum spectrum whose high-momentum components are suppressed compared to those in our model, the model will underestimate the fraction with three free protons and produce a corresponding increase in the two-proton cross section. The zero-threshold value for three free protons should be used with caution.

The most striking feature of the data is the relatively small fraction of the total absorption cross section with three-proton emission. The maximum cross section for three protons greater than 18 MeV is less than 15% of the estimated total; the fraction is only 2.5% for 50-MeV pions. These results appear to be evidence against a major role of ISI, as will be discussed in Sec. V.

B. Proton energy spectra

The observed spectra of protons are shown in Fig. 1 as a function of missing energy, i.e., zero energy corresponds to the case for which the total observed energy is equal to the kinetic plus mass energy of the incoming pion. The energies of particles other than protons are not included in these plots. All of the two-proton spectra show the same general features, namely (1) an easily distinguishable peak within 20 MeV of the pion total energy; (2) a second peak within 20 to 50 MeV of the total pion energy; (3) a less-distinct broad peak within 50 to 120 MeV of the total pion energy; and (4) a tail extending to the detection threshold (an observed energy of 44 MeV).

The first two features correspond respectively to quasideuteron absorption on a p-shell pair (the highest-energy peak), or to absorption on an s-shell pair or cross-shell absorption (the second peak). The cross section for absorption on a p-shell pair is within 10% of the free-deuteron absorption cross section. It was not possible to distinguish absorption on an s-shell pair from that with a single nucleon from each shell.

The third energy region has large contributions from processes that involve either an initial scattering of the pion followed by absorption or a scattering of one of the protons after the absorption. The lowest-energy region corresponds to three-body absorption, FSI, multiple interactions, or, for higher beam energies, to two-proton ejection without absorption. The importance of the

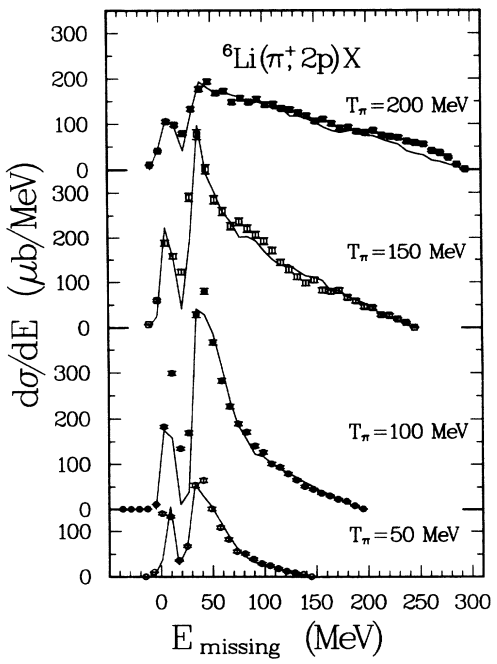

FIG. 1. Missing-energy distributions for two-proton final states. The solid line results from the fit with the phase-space model described in the text.

large-energy-loss region clearly increases with increasing pion energy. The question we will address in Sec. V is whether the increase is consistent with ISI/FSI.

The three-proton spectra shown in Fig. 2 peak about 40 MeV below the pion total energy. Since a minimum of 20 MeV is required to remove three protons from ^{6}Li, the peaks are about 20 MeV below the maximum available energy. The spectra also have tails dropping off smoothly to threshold, with no evident structure in them. As with the two-proton energy spectrum, there is also an increasingly large tail with increasing pion energy, although less pronounced than for the two-proton data.

The possibility that a substantial fraction of the three-proton final state was missed because a proton was at too forward an angle to be detected in the BGO ball could be checked by using the downstream detector sets. The total cross section for this process was obtained by integrating the average differential cross section for a forward proton detected in coincidence with two protons in the ball over the forward region not covered by the BGO. The results are given in Table III, along with the fraction of those events in which the two protons seen in the ball are "back-to-back", i.e., their opening angle is greater than 140° and the difference in their azimuthal angle is also greater than 140°, as determined from the centers of the hit detectors. The latter quantity relates to the issue of ISI followed by absorption, as will be discussed later. Even for 200-MeV pions, the "missing" cross section is only about one-third of the observed cross section for three protons in the ball. The final column lists the proton energy for a free πp scatter with the proton emitted at zero degrees.

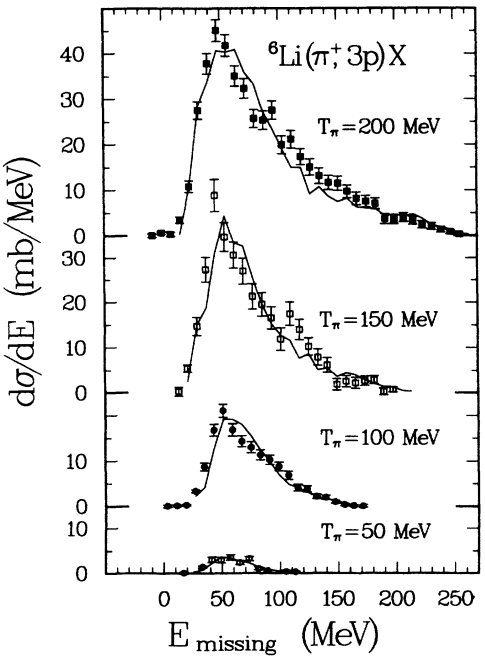

FIG. 2. Missing-energy distributions for three-proton final states. The solid line results from the fit with the phase-space model described in the text.

C. Other particles

As mentioned earlier, deuterons, neutrons, and low-energy charged particles are also seen in coincidence with the two- and three-proton events. There were no clearly identified ^{3}H, ^{3}He, or ^{4}He particles, as could be expected from the high energy required for their identification. Table II lists the observed cross sections for which two or three protons are in coincidence with various other particles, as well as the cross sections for one proton and one deuteron in coincidence. For comparison, we also list the cross sections for the $\pi 2p$ final state, and all final states with two or more charged particles (except pions) and at most one neutral, excluding those final states with two or more protons or one proton and one deuteron.

The total cross sections for the various combinations cannot be estimated for a variety of reasons. For the $2pn$ case, the neutron detection efficiency as a function of energy is not known, and we do not know the primary neutron energy spectrum. Much of the deuteron spectrum is below threshold and we have no measure of its shape. The low-energy charged-particle portion of the cross section is partially included in the cross-section estimates obtained with the lower proton-energy thresholds. However, without a knowledge of the particle type or the energy distribution in the lowest part of the spectrum, an accurate estimate of total cross section is not possible here either.

1. Neutrons

We can establish a lower limit of the cross section for the emission of energetic neutrons by estimating the detection efficiency from the known neutron-nucleus cross sections. For 100-MeV neutrons, about half will interact in the BGO, with about half of these arising from elastic scattering. We have required a neutral to have an observed energy of 18 MeV or more before it is called a neutron in order to eliminate low-energy photons and noise, as well as most elastically scattered neutrons in which the recoiling nucleus can give a small signal. Thus one would expect a maximum efficiency of about 25% at 100 MeV. The cross sections are nearly constant between 100 and 200 MeV, so one would not expect the efficiency to vary significantly for neutrons up to 200 MeV, although

TABLE III. Percentage of events with a forward proton and two protons in the ball which have QDA kinematics, total estimated cross section for a forward hit plus two protons in the BGO ball, and the energy of a proton at zero degrees resulting from a πp elastic scatter.

T_π (MeV)	QD	Total (mb)	E_p (mb)
50			25
100	20%	0.5	53
150	53%	0.9	83
200	54%	1.3	116

it would drop off rapidly at lower energies. Thus the physical $2pn$ cross sections are at least a factor of four greater than the observed value. As seen in Table II, the observed $2pn$ and $3p$ cross sections are nearly equal for the 200-MeV data, indicating that the physical $2pn$ cross sections are at least four times greater than the $3p$ cross sections. The observed $2pn$ cross sections fall off with decreasing pion energy. This behavior can be due to decreasing efficiency and/or decreasing cross section, although it is still half the $3p$ cross section for 150-MeV pions.

The $2pn$ cross section for 200-MeV pions is clearly large, but we must ask if it is in fact due to $2pn$ or if one is being misled by background, cross-talk between detectors, or charge exchange. For example, a high-energy proton might scatter out of one detector and into an adjacent one, where it would be identified as a neutral. The reaction $\pi^+ n \rightarrow \pi^0 p$ followed by absorption of the π^0 on a np pair would also lead to a $2pn$ final state.

The issue of background is easily addressed. Figure 3 shows the missing energy for two protons with the requirement of a neutron in coincidence, for 200-MeV π^+. A comparison with Fig. 1(d) clearly shows that most of the events are not accidentals, but in fact the summed energy of the protons peaks in the region of large missing energy. The fact that large energies are carried off by neutrons is indicated by the neutron energy spectrum for 200-MeV pions shown in Fig. 4. Because the observed energy is always less (and possibly much less) than the actual neutron energy, and we do not know the shape of the deposited energy spectrum as a function of neutron energy, it is not possible to infer the exact neutron energy spectrum. However, the fact that neutrons are observed up to energies of 190 MeV shows that high-energy neutrons are present. If the neutron energy is added to the summed proton energy in Fig. 3, the resulting spectrum is pushed toward the region of low missing energy. However, a sharp peak does not arise since much of the neutron energy is unobserved.

A comparison of the fraction of events with two adjacent detectors for the $3p$ final state, which should have little cross talk because of the requirement of both an E and ΔE signal, and the $2pn$ final state should indicate if cross talk is a problem. We find that 77% of the $3p$ events and 68% of the $2pn$ events do not contain two adjacent detectors, and the energy sum spectrum for those containing adjacent detectors does not look appreciably different from the spectrum for those not containing adjacent detectors, indicating that cross talk is not a significant source of false neutron signals.

The signature for charge exchange followed by absorption is less clear. However, in the pion energy range of this experiment, the $\pi^+ p$ cross section is four times larger than the charge-exchange cross section. Thus if scattering of the pion followed by absorption is important, one would expect the $3p$ cross section to be about four times larger than the $2pn$ cross section. That this is not the case implies that charge exchange followed by absorption cannot account for the large $2pn$ cross section.

2. Deuterons

The $2pd$ spectrum has a different character. The proton-energy sum shown in Fig. 5 for 200-MeV pions peaks at less missing energy than that for the neutron spectrum in Fig. 3. The deuteron energy spectrum at

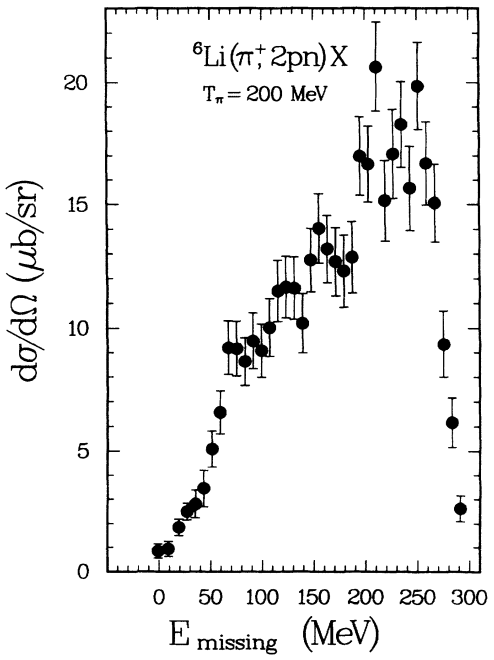

FIG. 3. Missing-energy distribution for the $2pn$ final state with 200-MeV pions.

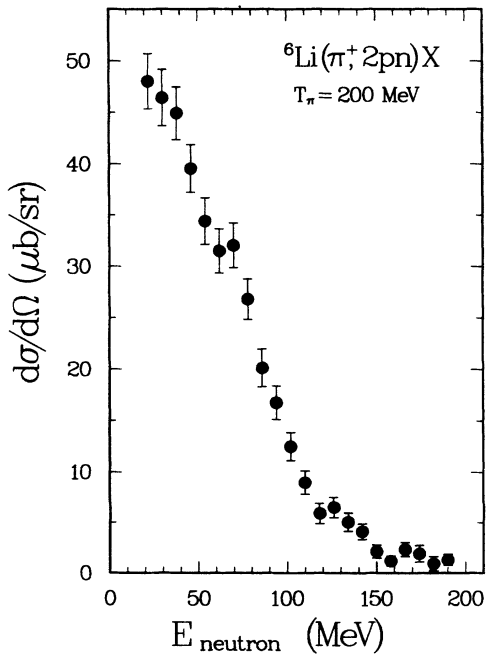

FIG. 4. Neutron energy spectrum for the $2pn$ final state with 200-MeV pions.

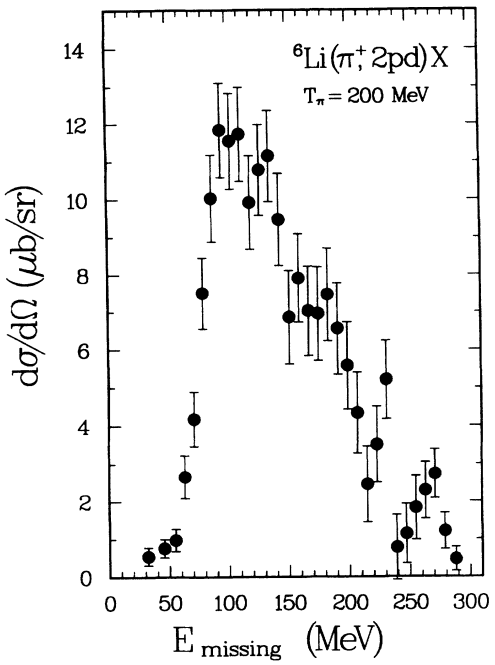

FIG. 5. Missing-energy distribution for the $2pd$ final state with 200-MeV pions.

200 MeV is shown in Fig. 6, along with a phase-space curve for the $2p2d$ final state, where one deuteron is assumed to have a Fermi-momentum distribution and the other a phase-space distribution (see Sec. IV). The solid curve shows the assumed Fermi-momentum distribution, taken from Ref. 28. The observed spectrum is between

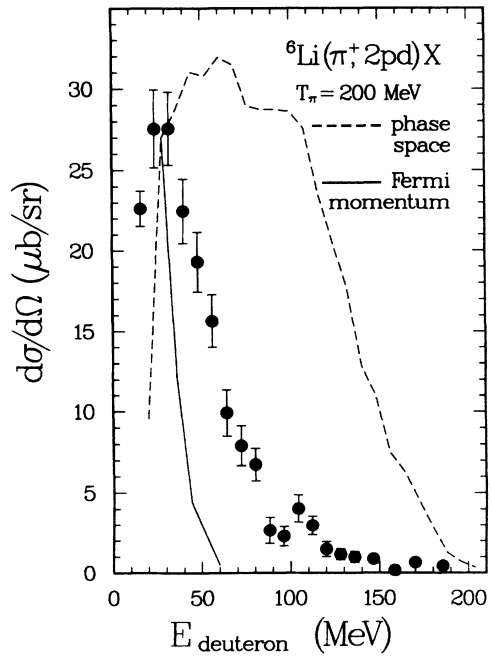

FIG. 6. Deuteron energy spectrum for the $2pd$ final state with 200-MeV pions. The dashed line represents the phase-space distribution of a $(2pd)d$ spectrum, and the solid line corresponds to an expected Fermi-momentum distribution.

the two curves, but clearly much closer to that with the Fermi-momentum distribution.

The energy sum of the two protons and the deuteron shows a definite peak near the maximum allowed energy. In contrast with neutrons, nearly the full deuteron energy spectrum is observed. Adding the deuteron energy to the two-proton energy sum gives a fairly sharp peak at low missing energy. We have shown the proton energy sum alone in order to compare it with the spectra in Fig. 1. The fraction of the $2p$ inclusive cross section seen as $2pd$, as well as the pd cross section, remains roughly constant as a function of energy. The angular distributions and correlations for the pd final state are similar to those of the two-proton final state. They are also similar to the results of Yokota,[17] all of which suggests that the pd yields result from absorption leading two protons followed by a neutron pickup.

For the data obtained at incident pion energies of 150 and 200 MeV, the observed two-proton energy spectra have missing energies so great that it is not possible to guarantee that the pion was absorbed. It is possible to estimate the importance of two-proton knockout without absorption by measuring the coincidence of two protons with a pion. That cross section was found to be 0.5 mb at 150 MeV and 1.4 mb at 200 MeV. Because most of the solid angle is covered, it is unlikely that the full cross section is much larger than the observed one. The summed energy spectrum falls in the region of the highest missing energy, as expected, with a maximum at a missing energy of about 240 MeV for 200-MeV pions. Even for the 200-MeV data, this reaction process appears to be responsible only for the region near the detection threshold and is thus not a major contributor to the observed two-proton cross section.

IV. PHASE-SPACE CALCULATIONS

In order to make a more quantitative interpretation of the underlying processes, we have attempted to describe the observed data with a series of phase-space calculations that embody various assumptions for the final states. Such a method allows us to estimate the undetected cross section due to missing-solid-angle and threshold effects, as well as to infer the contributions of different processes to the various parts of the two- and three-proton summed energy spectra and to tie together the magnitudes of these processes. Such interpretations have not been made in earlier work. We will thus be able to put tighter restrictions on the reaction mechanism than has been possible before. We shall describe our procedures in some detail in order to make the assumptions and methods clear.

The basic event generator was the phase-space program FOWL.[27] Since ^{6}Li has only 6 nucleons, all possible final states can be easily listed: $2p\alpha$, $2p^4$He*, $3pnd$, $2pdd$, $2pn^3$He, $3p^3$H, and $4p2n$. The phase-space distribution for each case can be weighted with the requirement that certain particles have a specified momentum distribution,

and by establishing correlations between particles.

In each case we make assumptions with regard to the number of "active" nucleons and require that the spectator particles have Fermi-momentum distributions. We have used the momentum distributions of Ref. 29 for the nucleons and of Ref. 28 for the heavier particles.

The active nucleons can be taken to have the angular distribution expected from QDA. For example, it is well known[17,19–23] that the two protons in the $2p\alpha$ case follow the angular distribution of the $\pi^+d \rightarrow 2p$ absorption rather closely, so we have weighted the phase-space calculations with this requirement.

The proper treatment for the cases with more than two free nucleons is less clear. We have attempted to model the QDA by generating the phase space with the spectators weighted to give a Fermi-momentum distribution. We then assume that the most energetic proton has an angular distribution characteristic of the $\pi^+d \rightarrow 2p$ reaction, but no angular requirement is made on the lower-energy protons.

We have also modeled final-state interactions by first generating a particular final state, then assuming that one of the active nucleons scatters from one of the "spectator" nucleons. The interacting pair is chosen by calculating the center-of-mass energy of each pair, then selecting among the pairs with a weight given by the free nucleon-nucleon total cross section at the center-of-mass energy. The pair is then scattered with an angular distribution given by the free cross section.

For example, in the case of the $3pnd$ final state we generate events in which one proton, the neutron, and the deuteron have Fermi-momentum distributions. The events are weighted to give the highest-energy proton an angular distribution corresponding to QDA. The two highest-energy protons are assumed to be the active pair. A center-of-mass energy is calculated for each proton paired with the low-energy proton and neutron. As described above, one pair is then chosen to "scatter," thus giving a set of events with a quasideuteron absorption followed by a final-state interaction.

This procedure models "hard" FSI, but does not include "soft" FSI.[10] However, a soft FSI does not lead to large energy transfer to the other nucleon and will not appear to populate the region of large missing energy. We have investigated this issue by requiring both particles in an np pair to have the same momentum. The energy sum in this case falls in about the same region as that for $3pnd$ with no FSI.

We can model three-body absorption by allowing three nucleons to have the distribution given by phase space, with the others weighted with Fermi-momentum distributions. We have neglected interactions with deuterons, ^{3}H, ^{3}He, or ^{4}He. Due to their relatively large mass, a nucleon scattering from them will not transfer as much energy as it would to another nucleon, and these events will not easily populate the regions of large missing energy.

We considered a number of combinations with or without the requirement of a QDA distribution and with or without FSI. The following sets were used for fitting the observed distributions: (a) $2p\alpha$, $2p^4$He*, $3pnd$, $2pn^3$He, and $3p^3$H with QDA distributions (which will be called $2p\alpha_{qd}$, $2p^4\text{He}^*_{qd}$, $3pnd_{qd}$, $2pn^3\text{He}_{qd}$, and $3p^3\text{H}_{qd}$); (b) $3pnd$, $2pn^3$He, $3p^3$H, and $4p2n$ with QDA distributions plus a final-state interaction (which will be called $3pnd_{qdfsi}$, $2pn^3\text{He}_{qdfsi}$, $3p^3\text{H}_{qdfsi}$, and $4p2n_{qdfsi}$); and (c) $2pn^3$He and $3p^3$H with a phase-space distribution of the nucleons, along with $4p2n$ in which three nucleons have Fermi momenta and three have a phase-space distribution, the latter occurring once for $2pn$ and once with $3p$ (which will be called $2pn^3\text{He}_{ps}$, $3p^3\text{H}_{ps}$, $2pn2pn_{ps}$, and $3pp2n_{ps}$). The $2p2d_{qd}$ channel was found to be essentially indistinguishable from $3pnd_{qd}$. For similar reasons the $3p^3\text{H}_{qd}$ channel was subsequently found to work best with nearly zero strength, and was thus discarded. The $2pn^3\text{He}_{ps}$, $3p^3\text{H}_{ps}$, $2pn2pn_{ps}$, and $3pp2n_{ps}$ cases will be used as models for three-body absorption; future reference to three-body absorption will mean these final states.

Once a basic event was generated, the behavior of the detector was simulated by estimating energy losses in the target, the probability of an interaction in the BGO, and losses due to the protons entering the support cans. Events with two hits in the same detector were eliminated since they would not be identified as protons. In this way the response of the detector to a known initial state could be investigated.

The corrections for nuclear reactions in the BGO have some uncertainty even if the magnitude of the nuclear reactions is known exactly. A proton that undergoes an inelastic scattering may lose enough energy as to fall outside the cuts in the particle-identification spectrum. The effect of this uncertainty was estimated on the basis of three different constraints: that no proton undergoing a nuclear reaction remained within the cuts, that all protons remained within the cuts, or that the energy loss was linear from 5 MeV up to the energy of the proton, checking whether the proton then remained within the cuts. The first two extreme cases varied from the intermediate third case by about 5% for 50-MeV incident pions, increasing to about 20% for 200-MeV pions.

The results of the above procedures were accumulated into two-proton and three-proton energy spectra for each final state and for each set of assumed constraints. Next, a set of possible final states was chosen. All of the final states of a given set that included three or more free protons were then normalized to fit the three-proton energy spectrum. Their normalization for the two-proton energy spectrum was thus fixed. Finally, all of the remaining states, i.e., those containing only two free protons, were normalized to fit the two-proton spectrum.

Although there appear to be many free parameters, there is in fact very little freedom in fitting the data. The energy sums for the different final states fall in different regions, thus limiting the degree to which they can be varied. The $2p\alpha$ state has a high energy sum and its normalization is nearly independent of the others.

The $3pnd_{qd}$, $2pdd_{qd}$, and $2pn^3He_{qd}$ states overlap with each other in the high-energy-sum (low-missing-energy) region, and the individual normalizations are not well determined. However, they have almost no overlap with the low-energy-sum (high-missing-energy) region. Other final states contribute to the low-energy region, but also to the three-proton spectrum. They cannot be freely adjusted to fit the two-proton spectrum without giving too large a contribution to the three-proton spectrum.

A. Comparisons with the data

As expected, there is no unique solution for the combinations of the various final states, and a number of combinations fit the observed energy spectra equally well. We have tried various combinations ranging from those that included none of the "three-body" absorption to as much three-body absorption as possible. In addition, for the 150-MeV and 200-MeV data, we have included the proton energy spectrum from the π^+pp final state as determined from those events in which all three particles were observed as another final state, also with an adjustable normalization. Nevertheless, for each combination tried, the low-energy-sum portion of the cross section could not be fitted without a substantial amount of the $2pn^3He$ final state, either as $2pn^3He_{qdfsi}$ or $2pn^3He_{ps}$.

As an example, we consider two extreme cases, i.e., those with no three-nucleon absorption and those with maximal three-nucleon absorption. The first case consists of the final channels $2p\alpha_{qd}$, $2p^4He^*_{qd}$, $3pnd_{qd}$, $2pn^3He_{qd}$, $3p^3H_{qdfsi}$, $2pn^3He_{qdfsi}$, $3pnd_{qdfsi}$, and $4p2n_{qdfsi}$, and the second consists of the $2p\alpha_{qd}$, $2p^4He^*_{qd}$, $3pnd_{qd}$, $2pn^3He_{qd}$, $3pnd_{qdfsi}$, $2pn^3He_{ps}$, $3p^3H_{ps}$, $3pp2n_{ps}$, and $2pn2pn_{ps}$ channels. We have included in the second case only the minimum number of final states which did not have a three-body phase space that were required to obtain a reasonable fit to the data. The $3pnd_{qd}$ channel in the first case was found to have negligible strength.

Both of these combinations resulted in reasonably good fits to the observed cross sections. The estimated total cross sections of the two cases agreed to within 10%. The results of the fits are summarized in Table IV. We have grouped the estimated total cross sections for the various final states in columns *A*–*E*, respectively: (*A*) "pure" QDA (the $2p\alpha_{qd}$ and $2p^4He^*_{qd}$ final states); (*B*) QDA with breakup of the residual nucleus, with or without FSI (those with the qd or qdfsi subscript, except $2pn^3He_{qdfsi}$ and those in column *A*); (*C*) the $3p^3H_{ps}$ state; (*D*) the $2pn^3He_{qdfsi}$ state; and (E) all three-body-absorption final states (those with the ps subscript) except for $3p^3H_{ps}$. The first value given in columns *A*, *B*, and *C* comes from the three-body-absorption combination, while the second is obtained from the no-three-body combination. The first value of the total cross section is the sum of columns *A*–*C* plus column *E*, and the second value is the sum of columns *A*–*C* plus column *D*. The two fits yield similar results for columns *A*, *B*, and *C*. The percentages listed are with respect to the estimated total cross section. Figures 7 and 8 show the two- and three-proton spectra at 200 MeV with the calculated distributions of sets *A*, *B*, *C*, and *E* for the maximal three-body combination.

As discussed earlier, different assumptions for the effects of nuclear reactions can change the corrected cross sections significantly, especially at higher energies. However, the ratios of the various parts change much less, with the ratio of columns *D* or *E* to the total changing by less than 10% even for 200-MeV incident pions.

The most evident feature of the analysis is the increasing fraction with pion energy of the total cross section found in either the $2pn^3He_{qdfsi}$ final state or the three-body-absorption final states. The three-body absorption is primarily due to $2pn^3He_{ps}$. The second evident feature is the smallness of the $3p^3H$ state. In Table V we compare the ratios of sets $A+B$, *D*, and *E* to the predicted values of the $\pi^+d \rightarrow 2p$ cross section. The cross section for the combination $A+B$ remains approximately constant at

TABLE IV. Estimated absorption cross sections from the two fits described in the text. The percentage is with respect to the estimated total cross section leading to two or more free protons. Columns *A*, *B*, and *C* are from the three-body-absorption fit (first value) and no-three-body-absorption fit (second value), *E* is from the three-body-absorption fit, and *D* is from the no-three-body-absorption case. The totals are for columns *A*, *B*, *C*, and *E* (first value of each column), and *A*, *B*, *C*, and *D* (second value). See text for complete description. The columns correspond to $A = 2p\alpha_{qd} + 2p^4He^*_{qd}$; $B = 3pnd_{qd} + 2pn^3He_{qd} + 3pnd_{qdfsi} + 3p^3H_{qdfsi} + 4p2n_{qdfsi}$; $C = 3p^3H_{ps}$; $D = 2pn^3He_{qdfsi}$; and $E = 2pn^3He_{ps} + 2pn2pn_{ps} + 3pp2n_{ps}$.

T_π (MeV)	*A* (mb)	*B* (mb)	*C* (mb)	*D* (mb)	*E* (mb)	Total (mb)
50	13/13	14/10	0.04/0.04	7.9	6.0	33/31
	38%	43%	0.1%	23%	18%	
100	14/14	27/26	0.15/0.15	19	14	55/59
	25%	49%	0.2%	32%	26%	
150	19/19	26/22	0.9	34	26	72/76
	26%	36%	1.3%	46%	36%	
200	11/12	19/19	1.7/1.7	33	30	62/66
	18%	31%	2.7%	51%	49%	

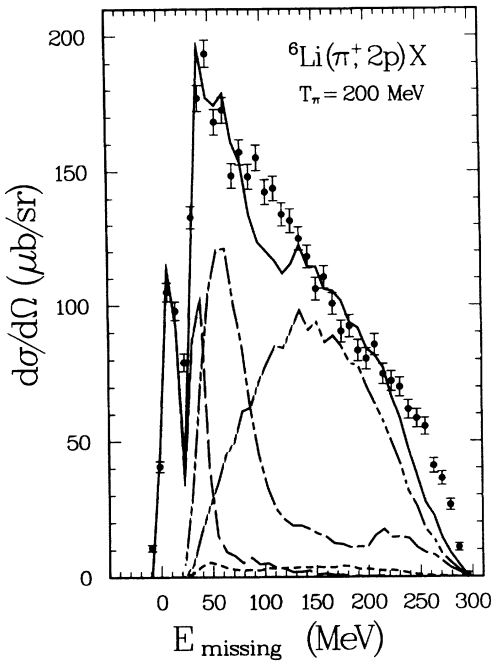

FIG. 7. Fits for the two-proton final state with 200-MeV pions obtained from the three-body-absorption calculation described in the text. The dashed line corresponds to pure QDA, the dot-dashed to QDA plus FSI, the dot-dot-dotted line to the $3p^3$H final state, and the dash-dot-dot-dotted line to three-body absorption. The solid line is the sum, with the $\pi 2p$ contribution omitted.

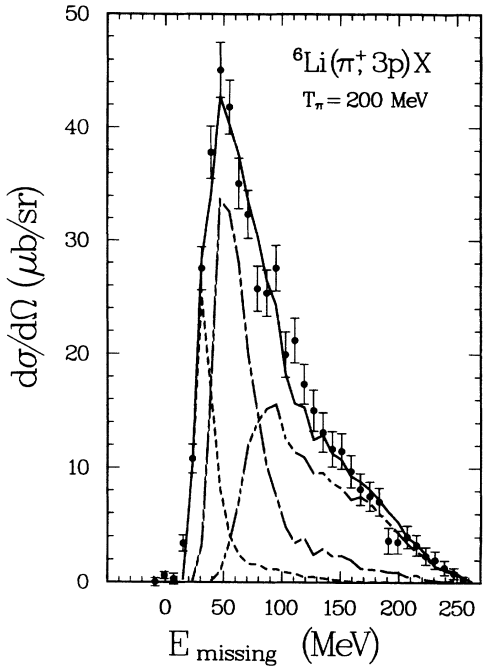

FIG. 8. Fits for the three-proton final state with 200-MeV pions obtained from the three-body-absorption calculation described in the text. The lines are the same as in Fig. 7.

four times the $\pi^+ d \rightarrow 2p$ cross section, while the other two ratios increase with increasing pion energy. Still, at this point it is not possible to draw any conclusions about three-body absorption.

We should comment that the method described here has a number of changes from the analysis presented in Ref. 15. In contrast to that analysis, we now include a correction for the $\pi 2p$ final state, additional final states, and fit both the three-proton and two-proton spectra simultaneously. We believe the changes result in a better estimate of the three-proton cross section that is seen as two protons. The effect of the additions was to decrease the total cross section slightly. In addition, the corrections for nuclear reactions in Ref. 15 assumed that no proton undergoing a nuclear reaction was identified as a proton after the reaction, which gives a larger cross section than that reported here.

Of course, more information is available than just the summed energy of the observed protons. In particular, one can also compare the Monte Carlo calculations with the single-proton energy distributions as a function of angle, and with the angular correlations between the two observed protons. If various models give different results for these quantities, it should be most evident in the regions of high missing energy, which is dominated by the final states resulting from FSI or three-body absorption.

B. Single-proton distributions

We consider first the single-proton energy spectra as function of angle. The BGO ball has poor angular resolution, so the spectra were simply divided into four angular bins which approximately covered the angles 25°–63°, 57°–108°, 94°–142°, and 135°–161°. There is some overlap between bins resulting from the shape of the crystals. For brevity, these four groups will be called row 1 (most forward) to row 4 (most backward).

TABLE V. Absorption cross sections on ^{4}He and ^{2}H, ratios of fitted cross sections to deuteron absorption cross sections, and pp and pn total cross sections for energies expected from QDA.

T_π (MeV)	^{4}He (mb)	$\pi^+ d \rightarrow 2p$ (mb)	$A + B/\pi d$	$D/\pi d$	$E/\pi d$	pp (mb)	np (mb)
50		5.9	4.6	1.3	1.0	35	90
100	76±12	10.6	4.3	2.0	1.3	32	76
150	76±15	11.8	3.8	3.2	2.2	30	73
200	52±17	7.4	4.3	4.9	4.0	28	61

The various final states fall into separate regions of summed energy. The highest-energy regions correspond to QDA, and the lower-energy regions to FSI or three-body absorption, or to π^+pp final states. Figures 9–12 show the inclusive single-proton cross sections $d\sigma^2/d\Omega\, dE$ from the ^{6}Li$(\pi, 2p)$ reaction for each of the angular bins with a high-energy cut on the total two-proton energy sum. The cut restricts the data to the region that would be dominated by a three-body absorption mechanism. Figures 13–16 show the same thing for the ^{6}Li$(\pi, 3p)$ reaction, with no cut on energy.

The fits for the two extreme cases of three-body absorption are very similar for 50- and 100-MeV pions. Both cases give a reasonably good description of the data for the two-proton final state, but slightly less so for the three-proton final state. For $T_\pi = 150$ MeV, the data are fitted better with maximal three-body absorption, especially at the more backward angles. By 200 MeV there is a clear difference between Figs. 12 and 16 with the case for maximal three-body absorption describing the data much better, particularly so for the most forward and most backward angles. However, the calculations for both cases give poor fits in the forward direction for the three-proton final state. This result seems consistent with the presence of an important component of ISI followed by absorption, which will be discussed in Sec. V B.

C. Angular correlations

Finally, we look at the angular correlations of the protons for the two-proton final states and compare them with the results calculated for the two extreme cases. We have again selected the energy region that should be dominated by three-body absorption. Figures 17–20 show the opening angle and the difference in azimuthal angle, as determined by the centers of the detectors, with

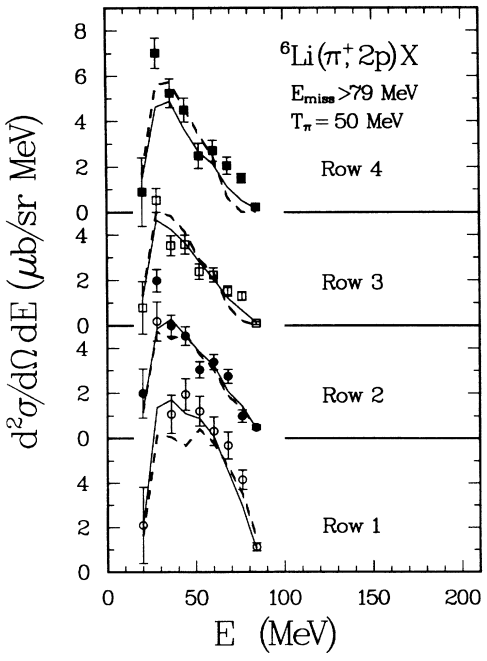

FIG. 9. Single-proton energy spectra as a function of angle for 50-MeV pions and for the two-proton final state with the constraint that the missing energy is greater than 79 MeV.

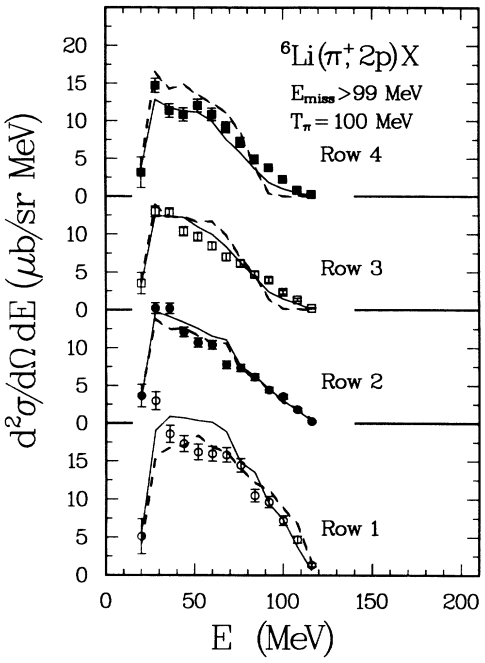

FIG. 10. Single-proton energy spectra as a function of angle for 100-MeV pions and for the two-proton final state with the constraint that the missing energy is greater than 99 MeV.

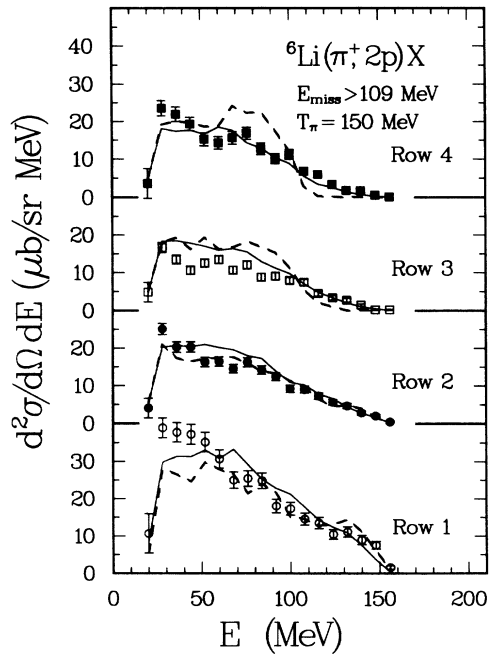

FIG. 11. Single-proton energy spectra as a function of angle for 150-MeV pions and for the two-proton final state with the constraint that the missing energy is greater than 109 MeV.

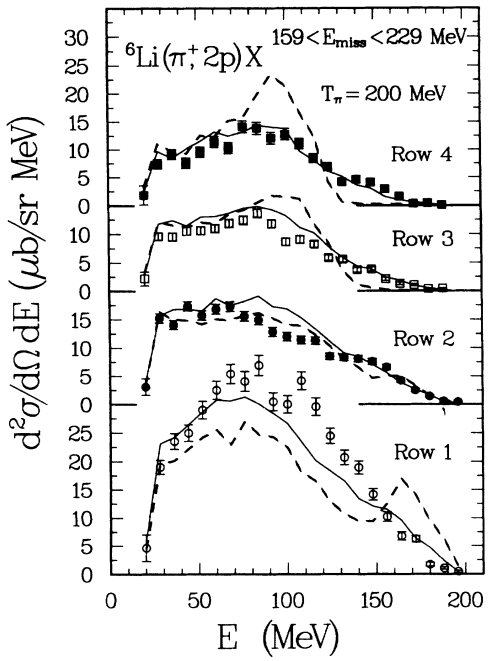

FIG. 12. Single-proton energy spectra as a function of angle for 200-MeV pions and for the two-proton final state with the constraint that the missing energy is between 119 and 229 MeV.

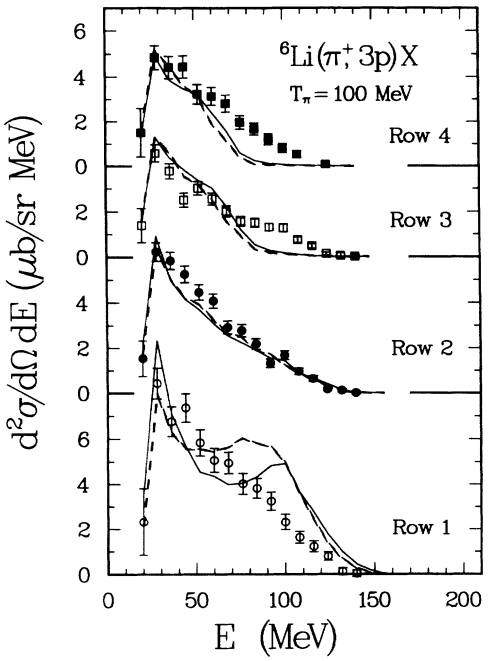

FIG. 14. Single-proton energy spectra as a function of angle for 100-MeV pions and for the three-proton final state with no energy cut.

a smearing corresponding to the detector resolution. As before, the solid and dashed lines indicate the cases for three-body absorption and for no-three-body absorption, respectively. The results of the models are not distinctly different at any energy. One sees, however, that a significant fraction of the data is not coplanar. For comparison, we also show the other energy bins for 150-MeV pions in Figs. 19(c)–(f). The highest-energy bin is distinctly coplanar and back-to-back, as expected from QDA with little other interaction.

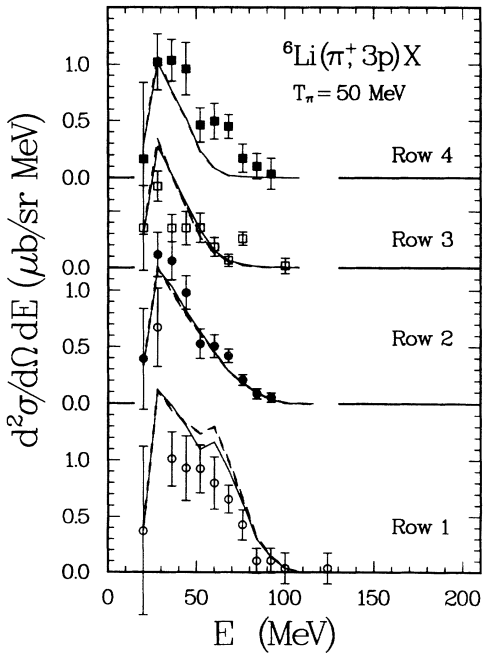

FIG. 13. Single-proton energy spectra as a function of angle for 50-MeV pions and for the three-proton final state with no energy cut.

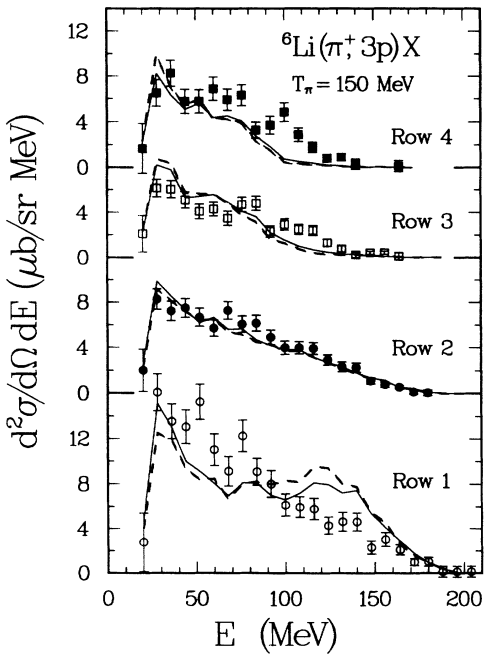

FIG. 15. Single-proton energy spectra as a function of angle for 150-MeV pions and for the three-proton final state with no energy cut.

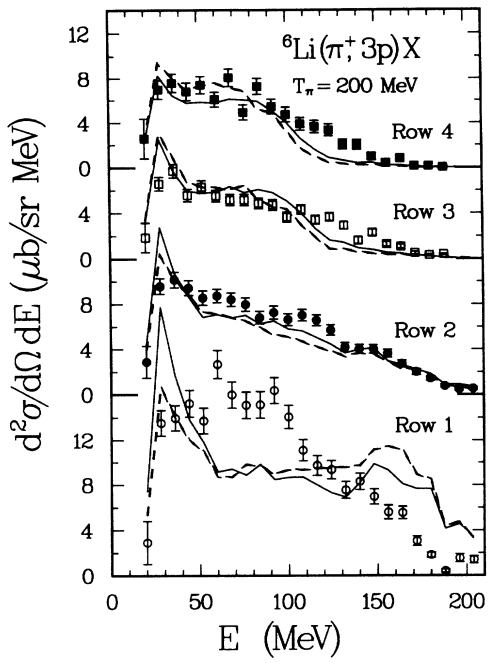

FIG. 16. Single-proton energy spectra as a function of angle for 200-MeV pions and for the three-proton final state with no energy cut.

V. ABSORPTION MECHANISMS

Although the differences in the fits are not very large, it appears that the data can be described slightly better with the assumption of maximal three-body absorption, particularly for the reactions with higher-energy pions. However, the differences are not large enough to make a convincing case for three-body absorption. We next examine the relative importance and energy dependence of the different components to see if a better distinction can be made.

A. Quasideuteron absorption with FSI

We first examine the case of QDA followed by FSI. As was discussed earlier, the portion of the cross section with large missing energy increases with the pion beam energy, both relative to the total two-proton cross section and to the deuteron-absorption cross section. Could this result be due to FSI?

Table V lists the free *pp* and *np* cross sections. The proton energies were taken to be those of the protons from the $\pi^+ d \rightarrow 2p$ reaction at 0° and 180°, with the *pp* cross sections corresponding to these energies then averaged. For example, for 50-MeV pions the forward and backward protons have energies of 120 and 67 MeV. The *pp* cross sections at these energies are 28 and 42 mb, with an average of 35 mb, the entry in the table.

It can be seen from Table V that, while the sum $A+B$ remains about 4 times as large as the free-deuteron cross section,[26] the values for D or E increase rapidly, more than doubling from 100 to 200 MeV. At the same time, the free NN cross sections decrease, particularly the *np* cross section, which decreases by 20% from 100 to 200 MeV. The D and E processes do not have the energy dependence that would be expected from FSI. In particular, their absolute magnitudes remain about constant from 150 to 200 MeV, even though the free-deuteron absorption cross section drops by 30%, and the free NN cross sections drop slightly. Such a behavior is difficult

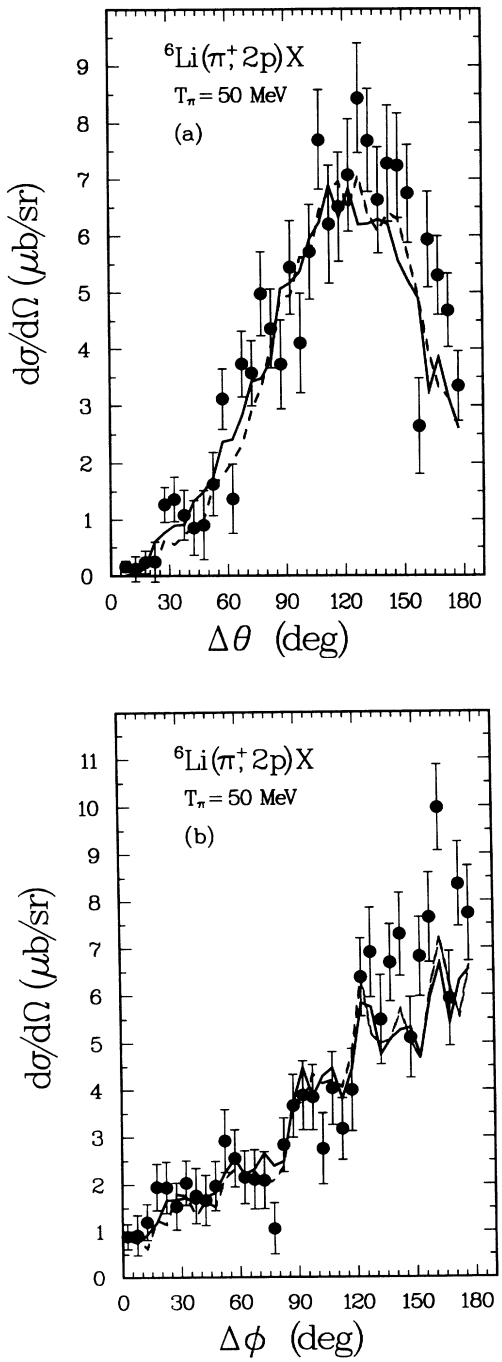

FIG. 17. Opening angle $\Delta\theta$ (a) and difference in azimuthal angle $\Delta\phi$ (b) between protons of the two-proton final state at 50-MeV pion energy and for missing energies greater than 79 MeV.

to reconcile with simple QDA followed by a single FSI.

It thus seems that the lower-energy part of the cross section cannot easily be explained by FSI. The proton-energy spectra and the dependence on angle instead resemble three-body absorption. The energy dependence of this part of the spectrum also becomes more important with increasing energy, although the free *np/pp* cross sections decrease.

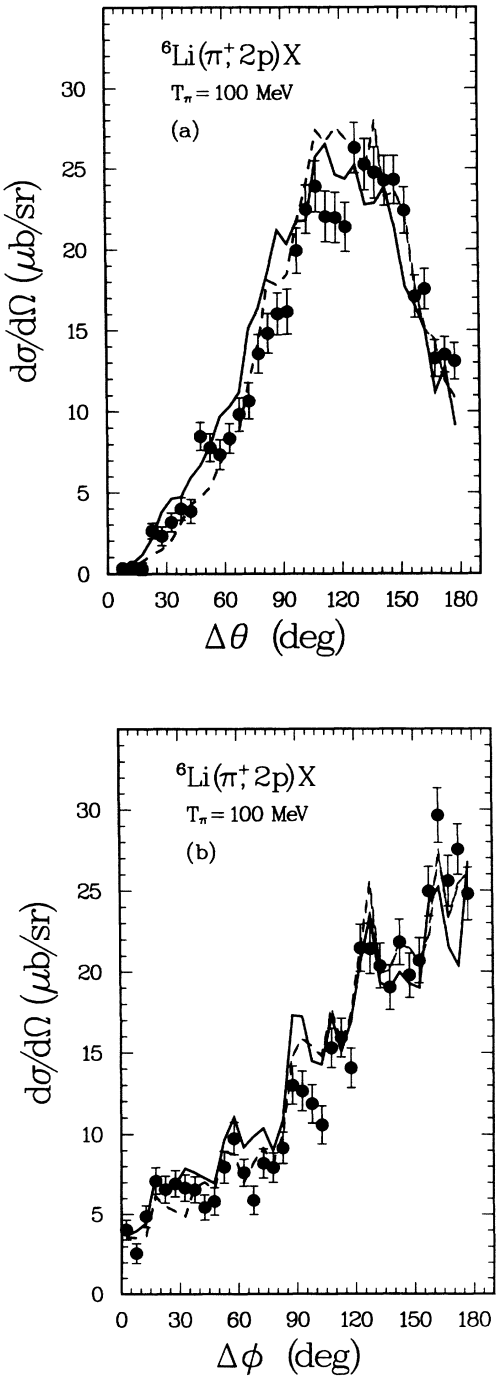

FIG. 18. Opening angle $\Delta\theta$ (a) and difference in azimuthal angle $\Delta\phi$ (b) between protons of the two-proton final state at 100-MeV pion energy and for missing energies greater than 99 MeV.

B. Quasideuteron absorption with ISI

Next we consider whether a scattering of the pion before absorption can lead to the large-energy-loss part of the spectrum. The signature for this process would be a scattering of the pion with large energy transfer to the nucleon, followed by absorption of the pion. Such a large energy transfer requires that the nucleon be scattered into the forward direction. In Table III, we list the maximum energy of the nucleon in a free πN scatter. The energies are generally too small to populate the region with the greatest missing energy. Fermi momentum of the struck nucleon can increase the energy transfer, but it is still unlikely to contribute to the region of large missing energy. We are not concerned here with ISI followed by QDA in which only relatively small energy is transferred to the recoiling proton, since that cannot affect the region of large energy loss.

At the energies of this experiment, π^+p elastic scattering is about nine times larger than π^+n elastic scattering, so one would expect that ISI followed by QDA would be seen mainly in the three-proton final state. One would expect the nucleons resulting from the absorption to be mainly back-to-back. However, we have seen that, even with a very forward proton, only about half of the events appear to have the kinematics expected for an ISI followed by a "pure" quasideuteron absorption.

This conclusion is consistent with the observed three-proton single-energy spectra seen in Figs. 13–16. At 150 and 200 MeV especially, the forward cross sections are enhanced over those expected from either FSI or three-body absorption in the most forward angles, for proton energies that correspond to quasi-elastic scattering. But the apparent ISI plus QDA does not dominate the three-proton spectrum even at the highest energy, where it is perhaps one-half the cross section. This low value is consistent with the results of Brückner *et al.*[4] on ^{12}C at 242 MeV, in which less than half of the three-proton spectrum appeared to be due to an ISI followed by absorption.

Thus, there is little direct evidence for significant cross section resulting from ISI with large energy transfer to the struck nucleon. The region of large missing energy is dominated by *ppn* rather than *ppp*, as would be the case if ISI is followed by absorption. All of these considerations indicate the low-energy part of the spectrum cannot be explained by a ISI plus QDA.

C. *ppn* triplet or *pnn* triplet

The next question concerns the relative importance of absorption on a *ppn* triplet versus a *pnn* triplet. A definitive answer to this issue cannot be given because, as we have seen, there is no unambiguous signature for three-body absorption at any energy. The strongest evidence for a three-body mechanism is in the large increase with energy of the cross section at large missing energies. Assuming that this behavior is due to three-body absorption, the data indicate that most of the three-body-like absorption is in the *ppn* final state.

According to our fits based on the maximum three-body absorption, absorption on a *ppn* triplet ranges from 6% of the absorption on a *pnn* triplet at 50 MeV to 14% at 200 MeV. This value is especially small because the $2pnd_{\mathrm{qdfsi}}$ final state describes the empirical three-proton spectra rather well. However, if we assume that all of the observed three-proton spectra are due to absorption on a *ppn* triplet, we find that it amounts to about 40% of the absorption on *pnn* triplets at 50 MeV, the value increasing to about 80% at 200 MeV. At 200 MeV, however, as much as one-half of the three-proton cross section could be due to ISI followed by two-body absorption. In that case, the ratio of *ppn* absorption to *pnn* absorption is about one-half. In both cases absorption on a *pnn*

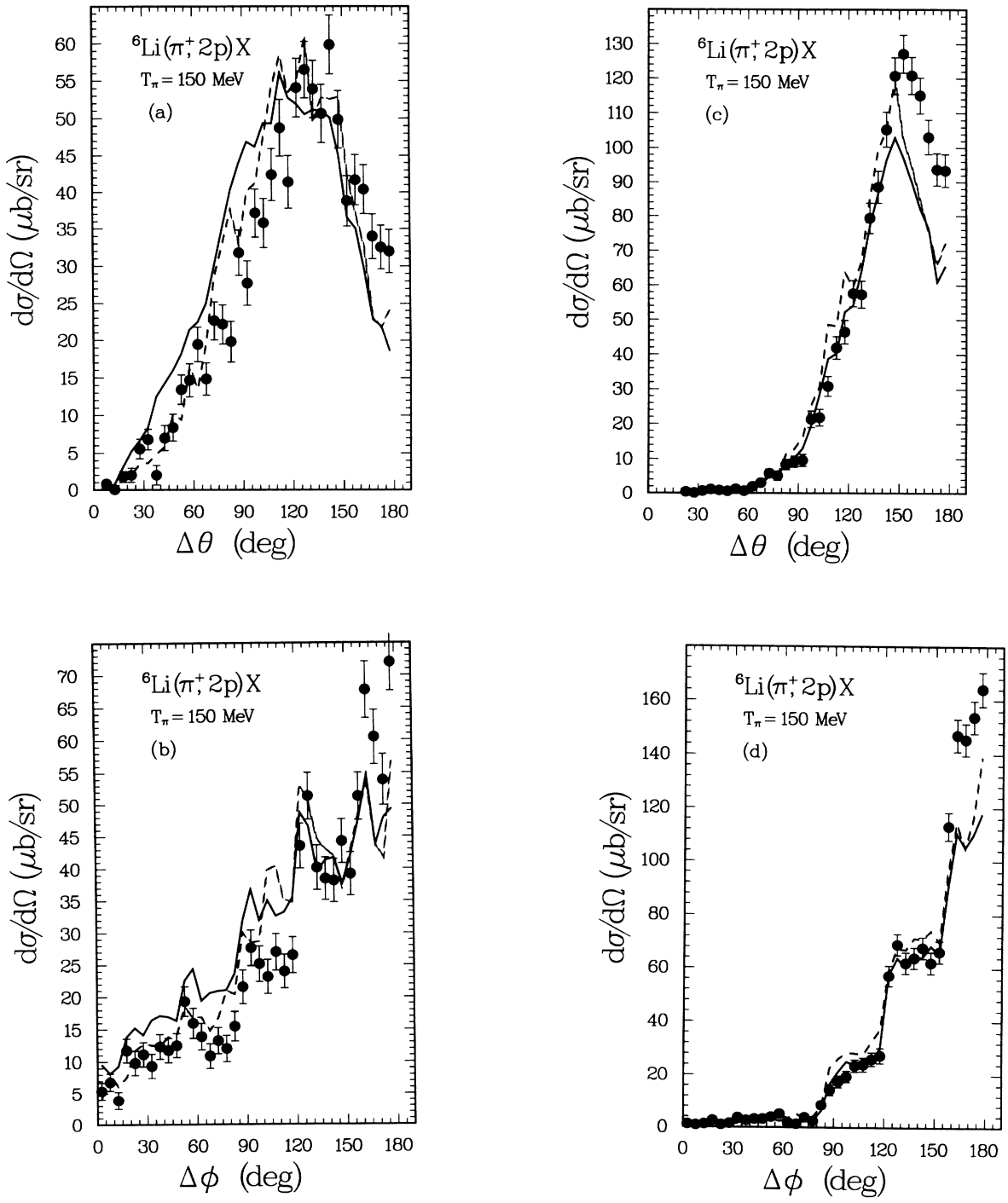

FIG. 19. Opening angle $\Delta\theta$ (a) and difference in azimuthal angle $\Delta\phi$ (b) between protons of the two-proton final state at 150-MeV pion energy and for missing energies greater than 109 MeV for (a) and (b), 49 to 109 MeV for (c) and (d), and less than 49 MeV for (e) and (f).

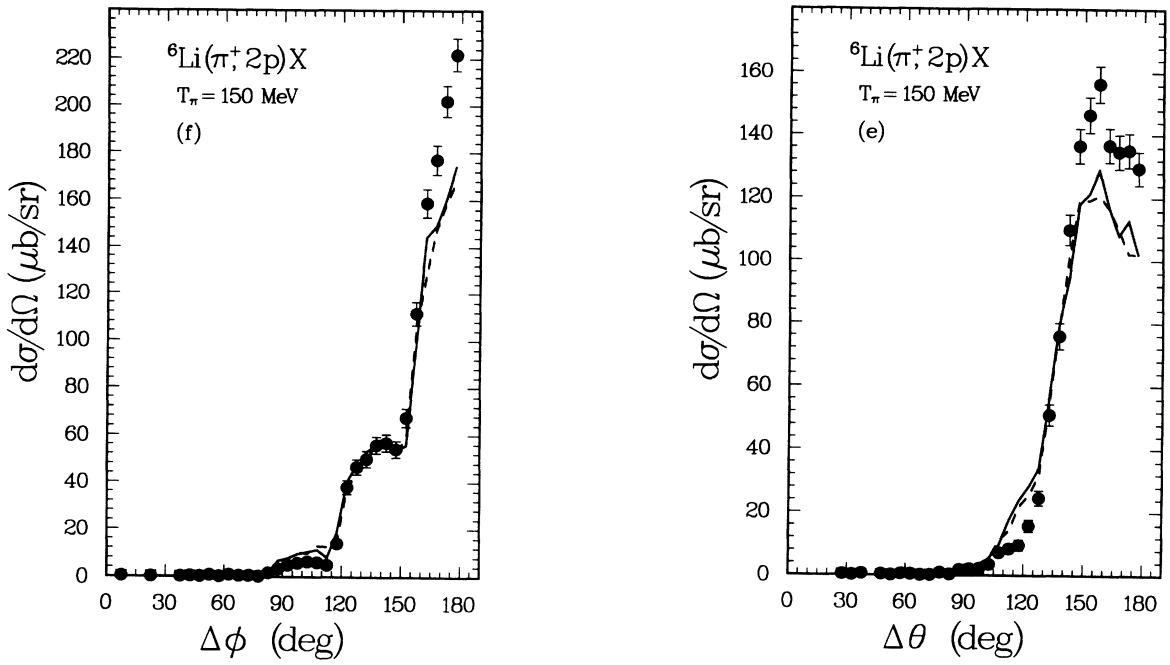

FIG. 19. (*Continued*).

triplet is larger than on a *ppn* triplet. These ratios differ slightly from those reported in earlier experiments, which found the two yields to be about equal in ^{3}He,[5,7] and the *ppn* absorption to be about one-half the *pnn* absorption in ^{4}He.[9]

Tacik *et al.*[3] measured pion absorption on ^{12}C leading to three-proton final states at 130, 180, and 228 MeV. They found the fraction of the total absorption on *ppn* triplets to be 4.6%, 11.1%, and 18.6%, respectively. For T_π = 150 MeV, we find about 20–30 % of the absorption on *pnn*, and less than 5-10 % on *ppn*, a result that does not disagree with the Tacik result. A calculation by Oset *et al.*[30] estimated the fraction of three-body absorption on ^{12}C to be about 30% at 150 MeV. When combined with the Tacik result, one finds the ratio of absorption on a *pnn* triplet to that on a *ppn* triplet to be about two, again in approximate agreement with our result.

Finally, we consider the possibility of four-body absorption, presumably on the ^{4}He core, resulting in a 3*pn* distribution. Our data do not require the presence of any four-body absorption, although it is not excluded either. Calculations of the phase-space distribution of 3*pnd* with a Fermi distribution of the deuteron momentum and no other restriction, fit to the three-proton data, show that a four-body absorption channel could be responsible for at most half of the three-proton yield, or 8% of the total cross section leading to two or more protons at 200 MeV and decreasing at lower energies. Thus, four-body absorption does not appear to be a significant component of the absorption cross section.

D. Summary of the phase-space section

Within the context of the model we have used, a substantial portion of the cross section appears to be due to a 2*pnX* final state, where *X* is unobserved and the three nucleons share the available energy. This process is well described in our model by the 2*pn*^{3}He final state. We note, though, that the 3*p*^{3}H final state does not have a significant cross section at any energy. Of course, the identification of the two states is not the same, as 3*p*^{3}H can be observed directly while the 2*pn*^{3}He is inferred from the shape of the large-missing-energy region and the small 3*p* cross section. It is equally possible that *X* could be *pd* or possibly 2*pn*, if the nucleons have a smaller fraction of high-momentum components than expected from electron scattering data.[29]

Another interesting result is the small difference of the angular distributions, especially for lower pion energies, between the QDA-plus-FSI and three-body-phase-space models for the interaction. Apparently, Fermi momentum coupled with a single scattering of a pair of nucleons fills the available phase space. Clearly, one cannot assume that a phase-space-like distribution automatically implies a three-nucleon absorption.

The model used does give a reasonably good description of the observed data. Thus we believe that the extrapolations of the observed data to the full solid angle and threshold are good to within the total estimated uncertainty of about 15%.

VI. COMPARISON WITH PREVIOUS DATA

The total cross sections estimated from the two- and three-proton data agree with the estimates obtained for natural lithium by Ashery *et al.*[31] who found a total of 44±20, 114±26, 124±30, and 59±33, at 85, 125, 165, and 205 MeV, respectively. Navon *et al.*[32] found a total cross section at 50 MeV of 28±21 mb for natural lithium. Our estimates at 50 and 200 MeV indicate that the nominal

values of Navon and Ashery are low, but that the uncertainties are large in each case.

A comparison with the ^{4}He absorption cross section[33] given in Table V with the estimates given in Table IV shows the two to be in approximate agreement, within the rather large uncertainties on both measurements. Therefore it does not appear that there is a significant increase in the cross section over that of ^{4}He, at least for the part leading to two or more energetic protons.

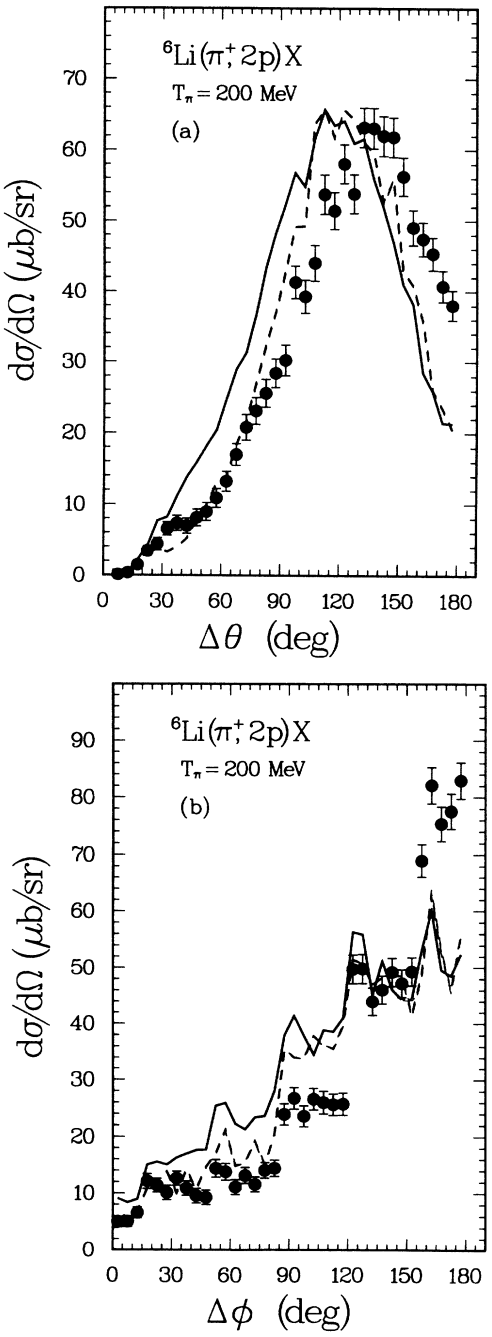

FIG. 20. Opening angle $\Delta\theta$ (a) and difference in azimuthal angle $\Delta\phi$ (b) between protons of the two-proton final state at 200-MeV pion energy and for missing energies between 119 MeV and 229 MeV.

Yokota *et al.*[17] measured two-proton coincidences on ^{6}Li at 70, 130, and 165 MeV in which the two protons were coplanar. The integrated cross section at 165 MeV was 25 mb and, by using an intranuclear-cascade code, they estimated the total two-proton cross section to be about 38 mb. Our fits to the 150-MeV data, with the solid angle and energy threshold comparable to the Yokota measurement, gives a coplanar cross section of about 20 mb, in agreement with their measurement. However our observed two-proton cross section, with no corrections, is already larger than their estimated total. The difference of a factor of 4 between the estimated total for final states with two or more protons and the coplanar cross section demonstrates the importance of noncoplanar measurements.

VII. SUMMARY AND CONCLUSIONS

The data show that a substantial portion of the absorption cross section, 20% at 50 MeV and nearly 50% at 200 MeV, is associated with a missing energy that would be expected if the pion energy were distributed among three nucleons, with one unobserved nucleon. The small cross section for three energetic protons and relatively large cross section for $2pn$ shows that the region of large missing energy is associated with a $2pn$ final state rather than $3p$. The behavior of this region is opposite to that expected from QDA followed by FSI. The observed cross section for $3p$ is too small, and the energy missing too large, for it to be explained by ISI. The ratio of $2pn$ to $3p$ is larger than would be expected from the free πp and NN cross sections. At higher energies, the angular distributions are more consistent with a phase-space distribution than with those expected from QDA with FSI. The ensemble of these observations gives strong evidence for an absorption mechanism involving three nucleons which cannot be explained as QDA with secondary interactions, and which becomes increasingly important with energy.

The mechanism for three-body absorption is not clear. Brown[34] has suggested a "double-delta" mechanism, in which the ΔN interaction gives rise to two deltas which then each decay via two-nucleon emission, resulting in four-nucleon absorption. However, this process is not expected to be important at lower energies, and our data do not support a four-nucleon absorption mechanism more significant than a few percent of the absorption cross section. Ashery[35] has proposed a model in which a πNN resonance is formed which then decays through three-nucleon emission. If the πNN resonance had isospin 1, the absorption on ppn triplets would be equal to the absorption on pnn triplets (as appears to be the case in ^{3}He), while if it had isospin 0, there would be no absorption on ppn triplets. The model of Oset[30] includes three-body absorption through successive and sequential interactions of the delta. This model predicts about the right cross section for three-nucleon absorption, but the isospin

dependence is not given. The energy dependence of the model does agree with our data and those of Smith.[11] It is also not clear whether a more sophisticated model of the interaction, such as that of Oset, can explain the observed ratio of the emission of two and three energetic protons, or the energy dependence in the region of large energy loss.

The experimental data here support the conclusion that a significant fraction of the absorption cross section is due to a three-body absorption mechanism, from about one-quarter at 50 MeV to one-half at 200 MeV. The nature of that mechanism is still unclear, in particular its isospin dependence.

ACKNOWLEDGMENTS

We should like to thank Lee Atencio for his help in the construction of the BGO ball, and Thomas Sommers and David Fox for their help with part of the analysis. This work was supported in part by the U.S. Department of Energy, the National Science Foundation, The Robert A. Welch Foundation, and NATO collaborative research Grant No. CRG890498.

*Present address: Fermi National Laboratory, Batavia, IL 60510.

†Present address: State University of New York, Stony Brook, NY 11794.

‡Present address: Lockheed Aircraft Corp., Palo Alto, CA 94304.

§Permanent address: Massachusetts Institute of Technology, Cambridge, MA 02319.

**Present address: Lyman Laboratory, Physics Department, Harvard University, Cambridge, MA 02138.

[1] R. D. McKeown, S. J. Sanders, J. P. Schiffer, H. E. Jackson, M. Paul, J. R. Specht, E. J. Stephenson, R. P. Redwine, and R. E. Segel, Phys. Rev. Lett. **44**, 1033 (1980).

[2] D. Ashery and J. P. Schiffer, Annu. Rev. Nucl. Part. Sci. 36, 207 (1986) gives an extensive review and reference list on pion absorption through mid 1986.

[3] R. Tacik, E. T. Boschitz, W. Gyles, W. List, and C. R. Otterman, Phys. Rev. C **32**, 1335 (1985); R. Tacik, E. T. Boschitz, W. Gyles, W. List, C. R. Otterman, M. Wessler, U. Wiedner, and R. R. Johnson, *ibid.* **40**, 256 (1989).

[4] W. Brückner, H. Döckner, H. Döbbeling, P. C. Gugelot, F. Güttner, H. Kneis, S. Majewski, M. Nomachi, S. Paul, B. Povh, R. D. Ransome, T.-A. Shibata, M. Treichel, Th. Walcher, P. Amaudruz, Th. Bauer, J. Domingo, R. Frey Q. Ingram, H. Jantzen, G. Kyle, D. Renker, and R. A. Schumacher, Nucl. Phys. **A469**, 617 (1987).

[5] K. A. Aniol, A. Altman, R. R. Johnson, H. W. Roser, R. Tacik, U. Wienands, D. Ashery, J. Alster, M. A. Moinester, E. Piasetzky, D. R. Gill, and J. Vincent, Phys. Rev. C **33**, 1714 (1986).

[6] R. A. Schumacher, P. A. Amaudruz, C. H. Q. Ingram, U. Sennhauser, H. Breuer, N. S. Chant, A. E. Feldman, B. S. Flanders, F. Khazaie, D. J. Mack, P. G. Roos, J. D. Silk, and G. S. Kyle, Phys. Rev. C **38**, 2205 (1988).

[7] G. Backenstoss, M. Iżycki, P. Salvisberg, M. Steinacher, P. Weber, H. J. Weyer, S. Cierjacks, S. Ljungfelt, H. Ullrich, M. Furić, and T. Petković, Phys. Rev. Lett. **55**, 2782 (1985).

[8] G. Backenstoss, M. Iżycki, P. Salvisberg, M. Steinacher, P. Weber, H. J. Weyer, S. Cierjacks, B. Rzehorz, H. Ullrich, M. Furić, T. Petković, and N. Simicevic, Phys. Rev. Lett. **59**, 767 (1987).

[9] G. Backenstoss, D. Brodbeck, M. Iżycki, P. Salvisberg, M. Steinacher, P. Weber, H. J. Weyer, A. Hoffart, B. Rzehorz, H. Ullrich, D. Bosnar, M. Furić, and T. Petković, Phys. Rev. Lett. **61**, 923 (1988).

[10] G. Backenstoss, M. Iżycki, R. Powers, P. Salvisberg, M. Steinacher, P. Weber, H. J. Weyer, A. Hoffart, B. Rzehorz, H. Ullrich, D. Bosnar, M. Furić, and T. Petković, Phys. Lett. B **222**, 7 (1989).

[11] L. C. Smith, R. C. Minehart, D. Ashery, E. Piasetsky, M. Moinester, I. Navon, D. F. Geesaman, J. P. Schiffer, G. Stephens, B. Zeidman, S. Levinson, S. Mukhopadhyay, R. E. Segel, B. Anderson, R. Madey, J. Watson, and R. R. Whitney, Phys. Rev. C. **40**, 1347 (1989).

[12] W. J. Burger, E. Beise, S. Gilad, R. P. Redwine, P. G. Roos, N. S. Chant, H. Breuer, G. Ciangaru, J. D. Silk, G. S. Blanpied, B. M. Preedom, B. G. Ritchie, M. Blecher, K. Gotow, D. M. Lee, and H. Ziock, Phys. Rev. Lett. **57**, 58 (1986); and W. J. Burger, Ph. D. thesis, Massachusetts Institute of Technology, 1985 (unpublished).

[13] B. G. Ritchie, N. S. Chant, and P. G. Roos, Phys. Rev. **C30**, 969 (1984).

[14] W. R. Gibbs and W. B. Kaufmann, in *Pion-Nucleus Physics: Future Directions and New Facilities at LAMPF*, Proceedings of the Los Alamos Conference, AIP Conf. Proc. No. 163, edited by R. J. Peterson and D. D. Strottman (AIP, New York, 1987).

[15] R. D. Ransome, V. R. Cupps, S. Dawson, R. W. Fergerson, A. Green, C. L. Morris, J. A. McGill, J. R. Comfort, B. G. Ritchie, J. Tinsley, J. D. Zumbro, R. A. Loveman, P. C. Gugelot, D. L. Watson, and C. Fred Moore, Phys. Rev. Lett. **64**, 372 (1990).

[16] H. Yokota, K. Nakayama, K. Ichimaru, T. Katsumi, T. Mori, S. Igarashi, K. Hama, R. Chiba, K. Nakai, J. Chiba, H. Enyo, S. Sasaki, T. Nagae, and M. Sekimoto, Phys. Rev. Lett. **57**, 807 (1986).

[17] H. Yokota, S. Igarashi, K. Hama, T. Mori, T. Katsumi, K. Nakayama, K. Ichimaru, R. Chiba, K. Nakai, and J. Chiba, Phys. Rev. C **39**, 2090 (1989).

[18] H. Yokota, S. Igarashi, K. Hama, T. Mori, T. Katsumi, K. Nakayama, K. Ichimaru, R. Chiba, K. Nakai, and J. Chiba, Phys. Rev. C, **40**, 270 (1989).

[19] T. Bressani, G. Charpak, J. Favier, L. Massonnet, W. E. Meyerhof, and C. Zupancic, Nucl. Phys. **B9**, 427 (1969).

[20] J. Favier, T. Bressani, G. Charpak, L. Massonnet, W. E. Meyerhof, and C. Zupancic, Nucl. Phys **A169**, 540 (1971).

[21] E. D. Arthur, W. C. Lam, J. Amato, D. Axen, R. L. Burman, P. Fessenden, R. Macek, J. Oostens, W. Shlaer, S. Sobottka, M. Salomon, and W. Swenson, Phys. Rev. C **11**, 332 (1975).

[22] R. Reider, P. D. Barnes, B. Bassalleck, R. A. Eisenstein, G. Franklin, R. Grace, C. Maher, P. Pile, J. Szymanski, W. R. Wharton, F. Takeutchi, J. F. Amann, S. A. Dytman, and K. G. R. Doss, Phys. Rev. C **33**, 614 (1986).

[23] G. Backenstoss, M. Iżycki, M. Steinacher, P. Weber, H.

J. Weyer, K. Von Weymarn, S. Cierjacks, S. Ljungfelt, U. Mankin, T. Petković, G. Schmidt, H. Ullrich, and M. Furić, Phys. Lett. **137B**, 329 (1984).
[24]D. Zhang, H. Breuer, N. S. Chant, B. S. Flanders, S. D. Hyman, D. J. Mack, P. G. Roos, J. D. Silk, K. Dhuga, G. S. Kyle, M. Wang, P.-A. Amaudruz, C. H. Q. Ingram, R. A. Schumacher, U. Sennhauser, J. Jacob, B. G. Ritchie, D. Rothenberger, J. McDonald, and A. Williams, Bull. Am. Phys. Soc. **34**, 1205 (1989).
[25]D. Rothenberger, B. G. Ritchie, J. R. Comfort, R. A. Giannelli, J. R. Tinsley, N. S. Chant, D. J. Mack, P. G. Roos, J. D. Silk, G. S. Kyle, M. Rawool, J. A. Escalante, and B. M. Preedom, Bull. Am. Phys. Soc. **34**, 1204 (1989).
[26]B. G. Ritchie, Phys. Rev. C **28**, 926 (1983).
[27]F. James, CERN Computer Center Program Library W515 (1975).
[28]A. Goldhaber, Phys. Lett. **53B**, 306 (1974).
[29]H. Hiramatsu, T. Kamae, H. Muramatsu, K. Nakamura, N. Izutsu, and Y. Watsae, Phys. Lett. **44B**, 50 (1973).
[30]E. Oset, Y. Futami, and H. Toki, Nucl. Phys. **A448**, 597 (1986).
[31]D. Ashery, I. Navon, G. Azuelos, H. K. Walter, H. J. Pfeiffer, F. W. Schlepütz, Phys. Rev. C **23**, 2173 (1981).
[32]I. Navon, D. Ashery, J. Alster, G. Azuelos, B. M. Barnett, W. Gyles, R. R. Johnson, D. R. Gill, and T. G. Masterson, Phys. Rev. C **28**, 2548 (1983).
[33]F. Balestra, S. Bossolasco, M. P. Bussa, L. Busso, L. Ferrero, D. Panzieri, G. Piragino, F. Tosello, I. V. Falomkin, V. I. Lyashenko, G. B. Pontecorvo, Yu. A. Shcherbakov, D. Cauz, R. Garfangnini, L. Santi, and A. Maggiora, Il Nuovo Cimento **92A**, 139 (1986).
[34]G. E. Brown, H. Toki, W. Weise, and A. Wirzba, Phys. Lett. **118B**, 39 (1982).
[35]D. Ashery, Phys. Rev. C **36**, 460 (1987).